Quantitative analysis of polarization behaviors of trion states in monolayer WS_2 in a magnetic field

Zijing Jin,[1] Baikui Li,[1,2,*] Guanghui Cheng,[1,3] Chengjie Zhou,[1] Hui Li,[1] and Jiannong Wang[1,†]

[1] *Department of Physics, The Hong Kong University of Science and Technology, Clear Water Bay, Kowloon, Hong Kong, China*

[2] *College of Physics and Optoelectronic Engineering, Shenzhen University, Nanhai Avenue 3688, Shenzhen, 518000 Guangdong, China*

[3] *Department of Physics, University of Science and Technology of China, Hefei, 230026 Anhui, China*

(Received 29 May 2022; revised 27 June 2023; accepted 2 November 2023; published 13 December 2023)

We investigated the polarization behaviors of the trion states in monolayer WS_2 via helicity-resolved magnetophotoluminescence spectroscopy under linearly polarized laser excitation. With nondegenerate electron densities, the magnetic field dependence of the polarization degree of the triplet trions ($P_{X_T^-}$) is positive and that of the singlet trions ($P_{X_S^-}$) is negative. With weak degenerate electron densities, both dependencies are positive. A positive (negative) dependence on the magnetic field indicates that the relative intensity of the low-energy (high-energy) component, i.e., circularly polarized emission from the K (K') valley, increases under a positive magnetic field. The magnetic-field and electron-density dependencies of $P_{X_T^-}$ and $P_{X_S^-}$ were well explained by using the scenario where a trion is a bound state of an exciton and an electron and taking into account the different valley polarizations of the excitons and the electrons due to the opposite energy shifts of the K and K' valleys in a magnetic field. We propose a model to quantitatively fit the magnetic field–dependent $P_{X_T^-}$ and $P_{X_S^-}$ with different electron densities by considering the nonhomogeneity of the electron distribution. Our findings provide insights into the underlying physics of trion formation.

DOI: 10.1103/PhysRevApplied.20.064023

I. INTRODUCTION

Monolayer (ML) transition-metal dichalcogenides (TMDCs) with a valley degree of freedom and reduced dielectric screening effect are ideal platforms to study the optovalleytronic physics and the properties of many-body excitonic states [1–9]. According to the selection rule, the excitonic states in the K (K') valley can be excited by or emit light with right-handed circular polarization σ^+ (left-handed circular polarization σ^-) [10–13]. Among the rich variety of excitonic states, the charged excitonic states, i.e., the trions, which carry the valley chiral information and can drift in an electric field, are attracting more attention for future development of optovalleytronic devices [14–16]. However, the formation or the configuration properties of the trions require further investigation [17–22].

Different models have been proposed to describe the formation and configuration of the trions. In a three-particle configuration model, a negative trion, which consists of two electrons and one hole, is formed in a bimolecular process in which a neutral exciton binds with a neighboring electron [17–19]. In a Fermi-polaron model, the trion represents the attraction state between the excitons and the Fermi sea [20,22]. In either model, the population of the trions depends on the population of the excitons and the electron density in corresponding valleys.

Under linearly-polarized-light excitation, equal populations of the excitonic states in the K and K' valleys will be generated. When a magnetic field is applied, the energy bands in the K and K' valleys shift oppositely due to different contributions from valley, spin, and orbital momentums [23,24]. This lifts the degeneracy of counterpart excitonic states, consequently leading to inequivalent populations of the counterpart excitonic states in the K and K' valleys according to the Boltzmann distribution function [3–5]. Meanwhile, the electron densities in the K and K' valleys also become different. In other words, nonzero valley polarizations of the excitonic states and the electrons can be generated simultaneously by applying a magnetic field. The valley polarization degree of the electrons can be further modified by applying a gate voltage to tune the background electron density. Therefore, investigation on the valley polarization behaviors of the trion states

*libk@szu.edu.cn
†phjwang@ust.hk

under magnetic fields can shed light on the formation and configuration properties of the trion states.

In this work, we investigated the polarization behaviors of the trions in ML WS_2 via helicity-resolved magnetophotoluminescence spectroscopy in out-of-plane magnetic fields under continuous-wave (cw) linearly polarized laser excitation. The polarization degree is defined as $P = (I(\sigma^+) - I(\sigma^-))/(I(\sigma^+) + I(\sigma^-))$, where $I(\sigma^+)$ and $I(\sigma^-)$ are the intensities of circularly polarized emission from the K and K' valleys, respectively. We observed that (i) the magnetic field dependence of the polarization degree of the triplet trions ($P_{X_T^-}$) is positive and the slope of the dependence becomes larger as the background electron density increases and (ii) the magnetic field dependence of the polarization degree of the singlet trions ($P_{X_S^-}$) is negative with nondegenerate electron densities and becomes positive with weak degenerate background electron density. We found that the magnetic-field and electron-density dependencies of $P_{X_T^-}$ and $P_{X_S^-}$ can be well explained in the bimolecular formation scenario from the evolution of valley polarizations of the neutral excitons and the electrons when a magnetic field is applied. A model is proposed to quantitatively fit the $P_{X_T^-}(B)$ and $P_{X_S^-}(B)$ characteristics by considering the nonhomogeneity of the electron distribution.

II. EXPERIMENTAL SECTION

A. Sample fabrication

The ML-WS_2 samples were prepared by a pickup technique in a nitrogen-filled glovebox [25,26]. Multilayer-BN flakes (10–30 nm thick), few-layer graphene flakes, and the ML-WS_2 flakes were first mechanically exfoliated onto different SiO_2/Si substrates. Polypropylene carbonate (15% concentration dissolved in anisole) spin-coated on a glass slide with a piece of polydimethylsiloxane stamp was used to pick up the flakes. For sample 1, a multilayer-BN flake, a ML-WS_2 flake, and a multilayer-BN flake were picked up in sequence and then transferred to another SiO_2/Si substrate. For sample 2, a multilayer-BN flake, a few-layer graphene flake, a ML-WS_2 flake, a multilayer-BN flake, and a few-layer graphene flake were picked up in sequence and then transferred to another SiO_2/Si substrate. Two electrodes were formed on the top and bottom few-layer graphene flakes by a standard electron-beam lithography technique.

B. Photoluminescence measurement

The micro-photoluminescence (PL) measurements were conducted in a 16-T physical property measurement system (PPMS, Quantum Design) equipped with an insert confocal microscope (Attocube). The sample was placed on a positioner stage (ANC 300). A cw 593-nm, 2.091-eV linearly polarized laser beam was introduced to the optical head by a polarization-maintained fiber (Thorlabs) and then was focused onto the sample surface by the $\times 100$ objective with a numerical aperture of 0.82. The PL signal was collected by another polarization-maintained fiber (Thorlabs) and recorded by an iHR 550 spectrometer (Horiba) with a charge-coupled device (Horiba). A long-pass filter (FF01-593/LP-25, Semrock) was used to filter the excitation laser beam in front of the spectrometer. For the polarization-resolved PL, a polarizer and a $\lambda/4$ waveplate were used for light detection with specified circular polarization.

We checked the polarization selection of the magnetophotoluminescence system by measuring both the polarized PL spectra of CdSe quantum dots (QDs) and the reflection of the laser. The QDs can be excited by the 593-nm, 2.091-eV laser. The PL of the QDs has a peak energy of 1.98 eV, which is close to that of the trion emissions of the WS_2 samples. Both the polarization degrees of the PL spectra of the QDs and the polarization of the reflected laser are close to zero under a magnetic field up to 16 T (see Fig. 5 in Appendix A). This suggests that the polarization distortion from the measurement system is negligible.

III. RESULTS AND DISCUSSION

Figure 1(a) shows the schematic structure of a ML-WS_2 sample (sample 1). The ML WS_2 was encapsulated with use of hexagonal boron nitride (h-BN). The positive direction of the magnetic field and the polarization directions of the excitation laser and PL emissions in detection are also illustrated. Unless stated elsewhere, all the PL spectra were measured at 10 K with use of a cw 593-nm, 2.091-eV excitation laser with linear polarization.

Figure 1(b) shows the σ^+ PL spectra of sample 1, i.e., right-handed-circularly-polarized-light emission from the K valley, under magnetic fields of −10, 0, and 10 T. In the PL spectrum at 0 T, multiple peaks can be identified according to the peak energies, binding energies of different excitonic states, and the temperature-dependent evolution of the PL spectra (see Fig. 6 in Appendix B). These peaks are emissions from neutral excitons (X) at 2.065 eV [3–5], neutral biexcitons (XD; a bright exciton bound with a dark exciton) at 2.049 eV, triplet trions (X_T^-) at 2.030 eV, singlet trions (X_S^-) at 2.025 eV [27–29], negative biexcitons (X^-D) at 2.011 eV [3–5,30–32], dark trions (D^-) at 2.006 eV [33–37] and its $K1$, Γ, and $K2$ phonon replicas (D_{K1}^-, D_Γ, and D_{K2}^-), at 1.96 eV, 1.967 eV and 1.984 eV, respectively [7,8,38–41], and the optically active recombination of dark trions (D_1^-) due to electron-electron scattering between the K and K' valleys at 1.993 eV [8]. The PL spectra are dominated by the emissions of negative excitonic states, while the relative intensities of neutral excitonic states are low. This is due to the natural electron doping of pristine ML WS_2 [2,15,42].

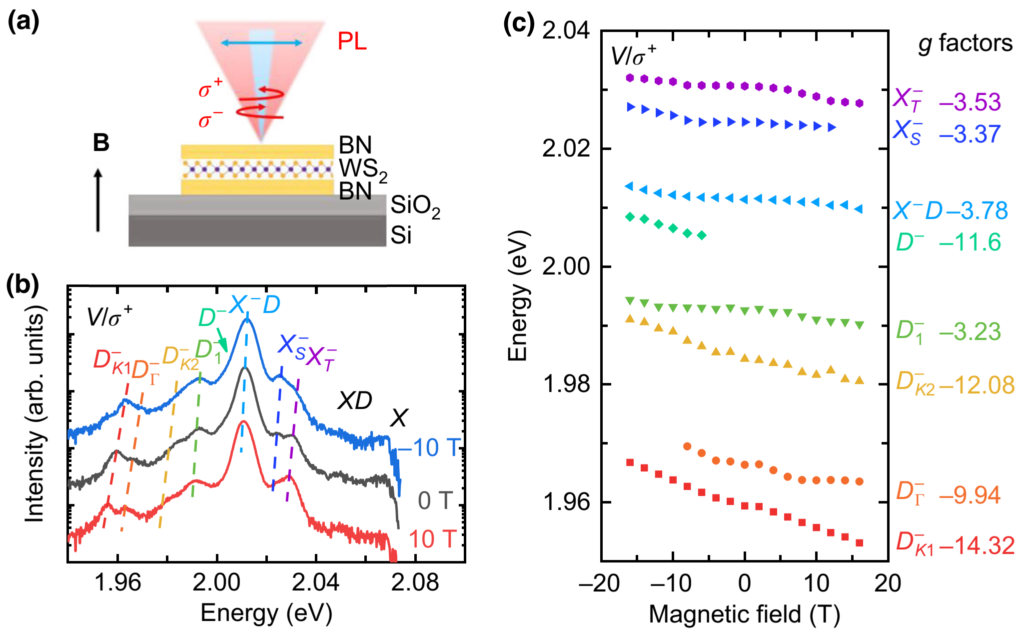

FIG. 1. (a) h-BN-encapsulated ML WS_2. The positive direction of the magnetic field **B** and the polarization directions of the excitation light and the PL light are also illustrated. σ^+ (σ^-) indicates the right-handed (left-handed) circularly-polarized-light emission from the K (K') valley. (b) σ^+ PL spectra of ML WS_2 under magnetic fields of −10, 0, and 10 T as indicated. The spectra are plotted with a logarithmic vertical scale and are vertically shifted for clarity. Multiple peaks can be identified with the notation labeled. The shift tendencies of the peaks are shown by the dashed lines. (c) Peak energies of the multiple emissions identified in the PL spectra as a function of the magnetic field. The corresponding g factors are given. The measurements were performed at 10 K.

In a magnetic field **B**, the energy bands of the K and K' valleys shift oppositely due to the valley Zeeman effect [24]. This leads to different energy shifts of the emission peaks of different excitonic states. The energy shift follows the equation $\Delta E = g\mu_B B$, where μ_B is the Bohr magneton and g is the g factor of the excitonic state. The peak energies in the PL spectra can be extracted by curve fitting using multiple Voigt functions (see Fig. 7 in Appendix C). Figure 1(c) shows the peak energies of the multiple peaks in the σ^+ PL spectra as a function of the out-of-plane magnetic field, from which the g factors are extracted and indicated. The g factors for the X^-_T, X^-_S, D^-_1, and X^-D peaks are −3.53, −3.37, −3.23, and −3.78, respectively. For D^- and its phonon replicas D^-_{Γ}, D^-_{K2}, and D^-_{K1}, the g factors are −11.6, −9.94, −12.08, and −14.32, respectively. All the g factors extracted in this work are consistent with those in previous studies [3,7,8,32,38,43–45]. This further verifies the assignments of the origin of the multiple emission peaks observed here.

The clear identification of different emission peaks allows us to investigate the polarization behaviors of the corresponding excitonic states. Here, we focus on the triplet trions and the singlet trions, both of which are bound states of neutral excitons and the electrons from the same valley or the other valley. Figure 2(a) shows the σ^+ and σ^- PL spectra in the trion emission range measured at 6 T (upper panel) and −6 T (lower panel). The dashed and dotted lines represent the decomposed X^-_T and X^-_S emission peaks, respectively. The evolutions of the σ^+ and σ^- PL spectra in the trion emission range under a magnetic field from −16 to 16 T are shown in Fig. 8 in Appendix D. Representative curve fittings of the PL spectra measured under other magnetic fields are shown in Fig. 9 in Appendix E.

Figure 2(b) shows the polarization degrees of X^-_T and X^-_S emissions as a function of the magnetic field. The polarization degree of an emission peak is defined as $P = (I(\sigma^+) - I(\sigma^-))/(I(\sigma^+) + I(\sigma^-))$, where $I(\sigma^+)$ and $I(\sigma^-)$ are the emission intensities when measured in σ^+ and σ^- detection configurations, respectively. As the magnetic field increases from −16 to 16 T, $P_{X^-_T}$ increases from −0.88 to 0.99, while $P_{X^-_S}$ decreases from 0.56 to −0.66. This reveals that $P_{X^-_T}$ ($P_{X^-_S}$) has a positive (negative) magnetic field dependence with a relatively large (small) magnitude of the slope. The positive (negative) dependence of the polarization degree on the magnetic field indicates that the low-energy (high-energy) component, i.e., σ^+ (σ^-) emission from the K (K') valley, is enhanced when a positive magnetic field is applied.

To understand the magnetic field dependencies of $P_{X^-_T}$ and $P_{X^-_S}$, the evolutions of the populations of trions with different valley configurations under magnetic fields need

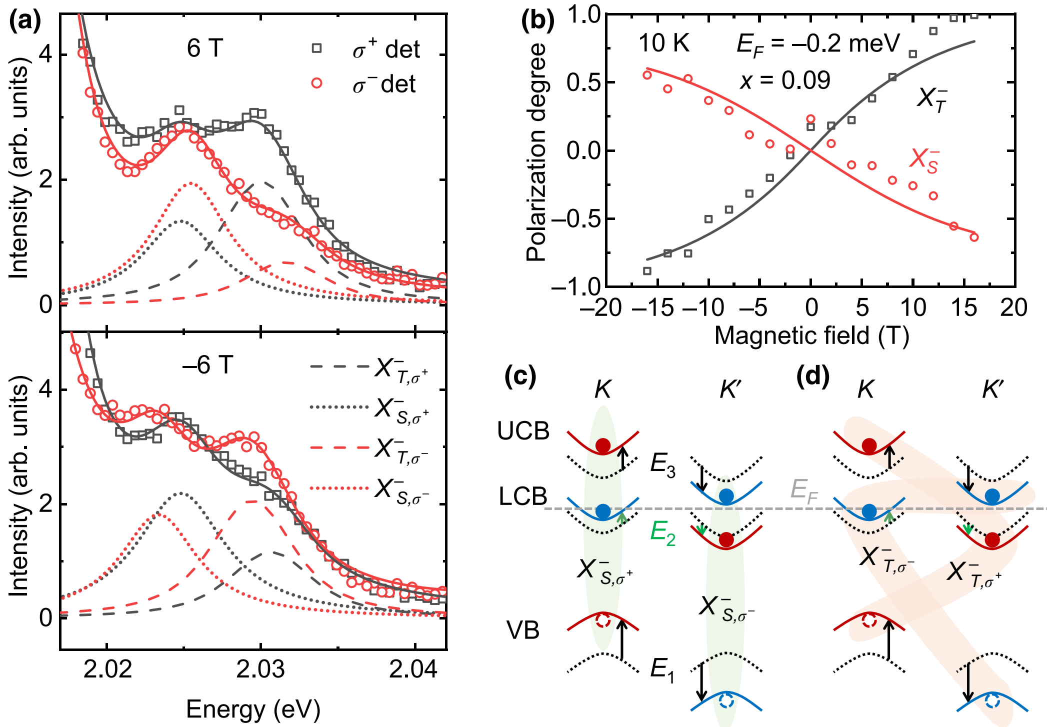

FIG. 2. (a) σ^+ (black squares) and σ^- (red circles) PL spectra of sample 1 in the trion emission range at 10 K under magnetic fields of 6 T (upper panel) and −6 T (lower panel). The solid lines are the fitting curves for the PL spectra obtained with use of multiple Voigt functions. The dashed (dotted) lines denote the decomposed X_T^- (X_S^-) emission peaks. (b) Polarization degree of X_T^- ($P_{X_T^-}$; black squares) and X_S^- ($P_{X_S^-}$; red circles) emissions at 10 K as a function of the magnetic field. The solid lines are fitting curves obtained with use of Eq. (5). (c),(d) Band diagrams and valley configurations of (c) X_S^- and (d) X_T^- in the K and K' valleys. The dashed lines represent the energy bands at 0 T and the solid lines represent the energy bands under a positive magnetic field. The horizontal dashed line denotes the equilibrium Fermi level E_F. The magnitudes of the energy shifts of the VB, LCB, and UCB in a positive magnetic field are denoted as E_1, E_2, and E_3, respectively. The lower valence band is not depicted for simplicity.

to be analyzed. Figures 2(c) and 2(d) illustrate schematically the valley configurations of X_S^- and X_T^-, respectively, in the K and K' band diagrams. The valence band (VB), the lower conduction band (LCB), and the upper conduction band (UCB) of the K and K' valleys under zero (a positive) magnetic field are represented by dotted (solid) lines. In the three-particle model, a singlet trion X_S^- (a triplet trion X_T^-) consists of a bright exciton and an electron in the LCB of the same valley (of the other valley). In the Fermi-polaron model, a singlet trion X_S^- (a triplet trion X_T^-) is the attraction state of the bright excitons and the electron Fermi sea in the LCB of the same valley (of the other valley).

At zero magnetic field, the electron densities in the K and K' valleys are equal. The total energies of the neutral excitonic states, triplet trions, and singlet trions with σ^+ and σ^- configurations are equal as well. In other words, the polarization degrees of the electrons, excitons, triplet trions, and singlet trions are zero under linearly polarized laser excitation at zero magnetic field. When a magnetic field is applied, the energy levels of the VB, the LCB, and the UCB of the K and K' valleys shift oppositely by $E_1 = 6\ \mu_B B$, $E_2 = 1.3\ \mu_B B$, and $E_3 = 4.2\ \mu_B B$, respectively [46,47]. The solid lines in Figs. 2(c) and 2(d) represent the shifted energy bands in a positive magnetic field, with E_1, E_2, and E_3 denoted by the arrows.

The opposite energy shifts of the energy bands in the K and K' valleys lead to (i) the redistribution of electrons in the K and K' valleys, consequently resulting in a nonzero polarization degree and (ii) the total-energies of the neutral excitons in K and K' valleys becoming different and consequently resulting in a net intervalley relaxation and a nonzero polarization degree. The intervalley relaxation rates of the trions are expected to be much smaller than those of the electrons and neutral excitons [48]. In the Fermi-polaron model, the intervalley relaxation of the "trions" is determined by that of the neutral excitons, while the change of the electron densities in different valleys has little influence on the populations of the "trions." Therefore, in either model, the intervalley relaxations of trions can be ignored.

The electron densities in the K and K' valleys under a magnetic field can be calculated. At zero magnetic field, the background electron densities in the K and K' valleys are equal and are denoted as n_0. The location of the Fermi level E_F at equilibrium at zero magnetic field is defined with respect to the LCB minimum. A positive (negative) E_F indicates that the Fermi level is above (below) the LCB minimum. When a positive magnetic field is applied, the LCB in the K valley shifts upward and that in the K' valley shifts downward. As a result, the electron density in the K valley decreases from n_0 to n_K, while that in the K' valley increases from n_0 to $n_{K'}$, where n_K and $n_{K'}$ are functions of the magnetic field and n_0 or E_F. Using the Fermi-Dirac distribution function, we can calculate n_K and $n_{K'}$ by

$$n_K = \int_{-E_F+E_2}^{-E_F+\Delta E_{\rm LCB}+E_2} \frac{D(E)}{e^{E/kT}+1} dE,$$
$$n_{K'} = \int_{-E_F-E_2}^{-E_F+\Delta E_{\rm LCB}-E_2} \frac{D(E)}{e^{E/kT}+1} dE, \quad (1)$$

where $\Delta E_{\rm LCB}$ is the bandwidth of the LCB, E_2 is the energy shift of the LCB, $D(E)$ is the density of states of the LCB, k is the Boltzmann constant, and T is the temperature. In Eq. (1), n_K and $n_{K'}$ depend primarily on the lower limits of the integration range. The upper limits of the integration range are far above the equilibrium Fermi level, resulting in a negligible effect on n_K and $n_{K'}$.

The relative populations of the neutral excitons in the K and K' valleys can also be estimated. In a positive magnetic field, due to the opposite shifts of the energy bands in the K and K' valleys, the total energy of the exciton in the K valley decreases and that in K' valley increases. The magnitude of the energy difference is $2(E_1 - E_3)$. In ML TMDCs, the intervalley relaxation of the neutral excitons is a primary process with a depolarization time less than 1 ps [49,50]. Therefore, supposing that the intervalley relaxation rate of the excitons is higher than the formation rate of the trions, the ratio of the exciton populations in the K and K' valleys can be estimated as $X_K/X_{K'} = e^{2(E_1-E_3)/kT} = e^{3.6\mu_B B/kT}$, according to the Boltzmann distribution function.

We now discuss the magnetic field–dependent polarization behaviors of the trions in ML WS_2 with different background electron densities under cw linearly polarized laser excitation.

(i) Nondegenerate regime, i.e., the Fermi level is below the LCB minimum at equilibrium. In this case, it is valid to use the bimolecular formation process and the three-particle configuration. It has been shown that the formation rate of the trion is greater than (or comparable with) the recombination rates of the excitons and the trions [51,52]. Therefore, under cw excitation, all the electrons can be bound with excitons to form the trions, and the populations of the trions with different valley configurations are primarily determined by the electron densities in corresponding valleys. Then, the polarization degrees of the singlet trions and triplet trions are given as

$$P_{X_S^-,1}(B) = \frac{X^-_{S,\sigma^+} - X^-_{S,\sigma^-}}{X^-_{S,\sigma^+} + X^-_{S,\sigma^-}} = \frac{n_K - n_{K'}}{n_K + n_{K'}},$$
$$P_{X_T^-,1}(B) = \frac{X^-_{T,\sigma^+} - X^-_{T,\sigma^-}}{X^-_{T,\sigma^+} + X^-_{T,\sigma^-}} = \frac{n_{K'} - n_K}{n_{K'} + n_K}. \quad (2)$$

It was shown above that $n_K < n_{K'}$ in a positive magnetic field. Therefore, Eq. (2) shows that $P_{X_S^-}$ and $P_{X_T^-}$ have negative and positive magnetic field dependencies, respectively, with equal magnitudes of the slopes. Equation (2) explains qualitatively $P_{X_S^-}(B)$ and $P_{X_T^-}(B)$ shown in Fig. 2(b). This indicates that sample 1 is in the nondegenerate-electron-density regime.

(ii) Weakly degenerate regime, i.e., the Fermi level is above the LCB minimum but still lower than that required to form a Fermi sea, or the LCB is partially occupied, even approaching the LCB minimum. In this case, the bimolecular formation process can still apply. However, the population of the trions is determined by both of the exciton density and the electron density. The polarization degrees of the singlet trions and triplet trions can be represented as follows:

$$P_{X_S^-,2}(B) = \frac{X^-_{S,\sigma^+} - X^-_{S,\sigma^-}}{X^-_{S,\sigma^+} + X^-_{S,\sigma^-}} = \frac{X_K n_K - X_{K'} n_{K'}}{X_K n_K + X_{K'} n_{K'}}$$
$$= \frac{(n_K/n_{K'})e^{3.6\mu_B B/kT} - 1}{(n_K/n_{K'})e^{3.6\mu_B B/kT} + 1},$$
$$P_{X_T^-,2}(B) = \frac{X^-_{T,\sigma^+} - X^-_{T,\sigma^-}}{X^-_{T,\sigma^+} + X^-_{T,\sigma^-}} = \frac{X_K n_{K'} - X_{K'} n_K}{X_K n_{K'} + X_{K'} n_K}$$
$$= \frac{(n_{K'}/n_K)e^{3.6\mu_B B/kT} - 1}{(n_{K'}/n_K)e^{3.6\mu_B B/kT} + 1}. \quad (3)$$

Under a positive magnetic field, we have $e^{3.6\mu_B B/kT} > (n_{K'}/n_K) > 1$. Equation (3) shows that both $P_{X_S^-}$ and $P_{X_T^-}$ have positive magnetic field dependencies and that the magnitude of $P_{X_S^-}$ is always smaller than that of $P_{X_T^-}$ in the weakly degenerate regime. This cannot explain the negative magnetic field dependence of $P_{X_S^-}$ shown in Fig. 2(b). Nevertheless, Eq. (3) predicts that the electron-density dependence of $P_{X_S^-}$ is more pronounced than that of $P_{X_T^-}$. This is because that as the Fermi level increases, $n_K/n_{K'}$ increases and gets closer to 1 due to the Fermi-Dirac distribution of the electrons in this regime.

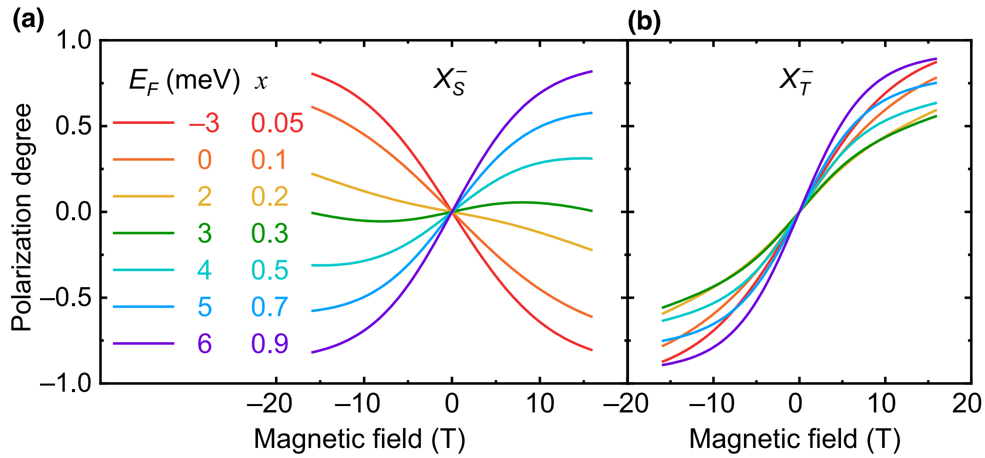

FIG. 3. Calculated polarization degrees of (a) the singlet trions X_S^- and (b) the triplet trions X_T^- obtained with Eq. (5) with different values of x and $E_{\rm F}$ as indicated.

(iii) Degenerate regime, i.e., the Fermi level is above the LCB minimum, and the Fermi-polaron scenario needs to be adopted. Here we assume that when the Fermi level is above the LCB minimum by more than 10 meV we need to apply the Fermi-polaron scenario [20].

In a Fermi-polaron model, the "trions" are the attractive coupling states of excitons with a Fermi sea of electrons [20,22]. At moderate carrier density, the emission intensity of the attractive mode or the populations of the "trions" are primarily determined by the populations of the excitons. Then, $P_{X_S^-}$ and $P_{X_T^-}$ under magnetic fields can be represented as follows:

$$P_{X_S^-,3}(B) = \frac{X_{S,\sigma^+}^- - X_{S,\sigma^-}^-}{X_{S,\sigma^+}^- + X_{S,\sigma^-}^-} = \frac{e^{3.6\mu_B B/kT} - 1}{e^{3.6\mu_B B/kT} + 1},$$
$$P_{X_T^-,3}(B) = \frac{X_{T,\sigma^+}^- - X_{T,\sigma^-}^-}{X_{T,\sigma^+}^- + X_{T,\sigma^-}^-} = \frac{e^{3.6\mu_B B/kT} - 1}{e^{3.6\mu_B B/kT} + 1}. \quad (4)$$

In this scenario, $P_{X_S^-}$ and $P_{X_T^-}$ are always equal with positive magnetic field dependence. Obviously, Eq. (4) cannot be used to explain the polarization behaviors of the trions of sample 1 shown in Fig. 2(b). This is expected because the electron density in our pristine ML WS_2 is not large enough to form a Fermi sea.

On the basis of the above discussions, we can see that the formation of trions in sample 1 can be described with use of the bimolecular model. To quantitatively analyze the magnetic field–dependent polarization degrees of the trions, we propose a model by considering the possible disorder-induced nonhomogeneous distribution of the electron density in the ML TMDCs [53,54]. It is reasonable to conjecture that in the nondegenerate regime the formation or the population of the trions is primarily determined by the populations of electrons, while in the weakly degenerate regime with relatively high electron density, it is determined by the populations of electrons and excitons. Then the magnetic field–dependent $P_{X_S^-}$ and $P_{X_T^-}$ can be represented by linear combination of Eqs. (2) and (3) with an empirical weighting parameter x as follows:

$$P_{X_S^-}(B) = (1-x)P_{X_S^-,1}(B) + xP_{X_S^-,2}(B),$$
$$P_{X_T^-}(B) = (1-x)P_{X_T^-,1}(B) + xP_{X_T^-,2}(B). \quad (5)$$

The physical meaning of the parameter x in Eq. (5) is clear. For the same sample, a larger x is expected with increasing electron density. For different samples with the same average electron density, a larger x indicates higher nonhomogeneity of the electron distribution.

As shown in Fig. 2(b), the magnetic field–dependent $P_{X_S^-}$ and $P_{X_T^-}$ of sample 1 can be well fitted with use of Eq. (5) with $x = 0.09$ and $E_F = -0.2$ meV. To further reveal the polarization behaviors of the singlet trions and triplet trions, we calculated $P_{X_S^-}(B)$ and $P_{X_T^-}(B)$ using Eq. (5) with different electron densities or E_F as shown in Figs. 3(a) and 3(b), respectively. As the electron density or E_F increases from -3 to 6 meV, the slope of $P_{X_S^-}(B)$ evolves from negative to positive, while that of $P_{X_T^-}(B)$ remains positive with a minimum. These behaviours can be explained intuitively by considering the contributions of the valley polarizations of the electrons and the excitons. Under a positive magnetic field, the valley polarization of the electrons is negative and that of the excitons is positive. The negative electron polarization contributes negatively to $P_{X_S^-}$ and positively to $P_{X_T^-}$. On the other hand, the positive exciton polarization contributes positively to both $P_{X_S^-}$ and $P_{X_T^-}$.

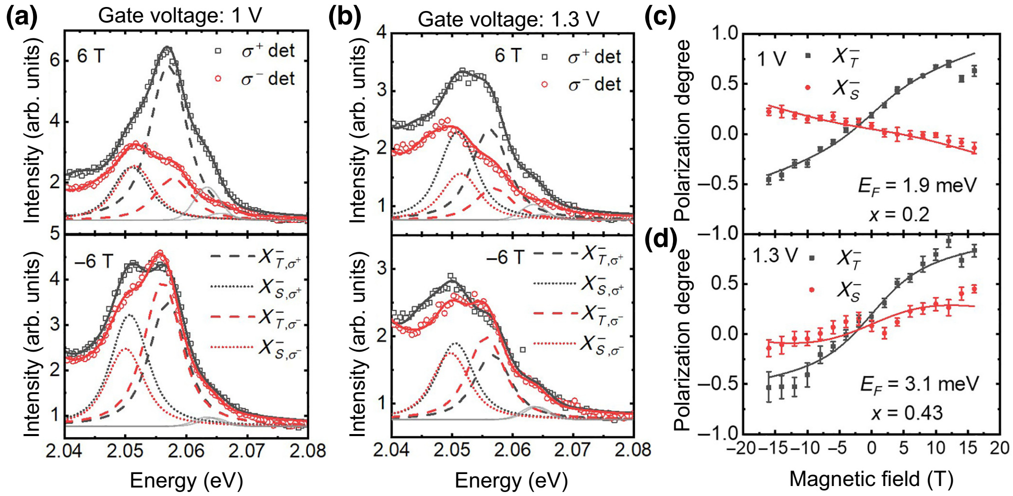

FIG. 4. (a),(b) σ^+ (black squares) and σ^- (red circles) PL spectra of sample 2 in the trion emission range with applied gate voltages of (a) 1 V and (b) 1.3 V. The upper (lower) panels show the PL spectra measured under a magnetic field of 6 T (−6 T). The solid lines are the fitting curves of the PL spectra obtained with use of multiple Voigt functions. The dashed (dotted) lines denote the fitted X_T^- (X_S^-) peaks. The gray lines denote the fitted biexciton emission peaks. (c),(d) Polarization degree of X_T^- emissions (black squares) and X_S^- emissions (red circles) as a function of the magnetic field at gate voltages of (c) 1 V and (d) 1.3 V. The solid lines are fitting curves obtained with Eq. (5) with the fitting parameters indicated.

At a relatively small E_F (less than 2 meV), the polarizations of the trions are dominated by the polarization of the electrons, which means that $P_{X_S^-}$ is negative and $P_{X_T^-}$ is positive. When E_F increases, the magnitude of the polarization of the electrons decreases, leading to a decrease of the magnitudes of $P_{X_S^-}$ and $P_{X_T^-}$. As E_F (greater than 3 meV) or the electron density further increases, the valley polarization of excitons becomes dominating in the trion formations. Then, the $P_{X_S^-}$ becomes positive and increases, while the $P_{X_T^-}$ remains positive and increases from a minimum value.

To verify the quantitative model proposed above, we fabricated a gated WS_2 sample (sample 2). The schematic cross-section structure, the gate-leakage characteristic, and the PL spectra of sample 2 are shown in Fig. 10 in Appendix F. Figures 4(a) and 4(b) show the PL spectra of sample 2 in the trion emission range measured in σ^+ and σ^- configurations under magnetic fields of 6 T (upper panel) and −6 T (lower panel) at a gate voltage of 1 and 1.3 V, respectively. The decomposed triplet and singlet trion emission peaks are plotted with dashed and dotted lines, respectively. The gray lines represent the decomposed biexciton emission peaks. Note that the emission energies of excitonic states in sample 2 are approximately 25 meV larger than those in sample 1 due to different dielectric environments. Coincidently, the high-energy side of the biexciton emission of sample 2 is attenuated by the long-pass filter used to filter the excitation laser beam (see Sec. 2). This leads to a shift toward the low-energy side of the biexciton emission peak, which is seen as a shoulder at about 2.065 eV in the recorded PL spectra. Nevertheless, the trions' emission is in the transmission range of the filter and the extraction of individual trion emission peaks is reliable.

Figures 4(c) and 4(d) show $P_{X_T^-}$ and $P_{X_S^-}$ of sample 2 as a function of the magnetic field at gate voltages of 1 and 1.3 V, respectively. At a gate voltage of 1 V, the magnetic field dependence of $P_{X_T^-}$ is positive and that of $P_{X_S^-}$ is negative. The magnitude of $P_{X_S^-}$ is smaller than that of $P_{X_T^-}$. These results are qualitatively the same as the results for sample 1. As the gate voltage increases to 1.3 V, the background electron density increases and E_F becomes higher. The magnetic field dependence of $P_{X_T^-}$ remains positive with a larger slope. Meanwhile, the magnetic field dependence of $P_{X_S^-}$ has changed to positive. These characteristics verify the calculated results and discussion presented above.

As shown by the solid lines in Figs. 4(c) and 4(d), $P_{X_T^-}$ and $P_{X_S^-}$ as a function of the magnetic field at different gate voltages can be well fitted with use of Eq. (5). The fitting parameters are $E_F = 1.9$ meV and $x = 0.2$ at a gate voltage of 1 V, and $E_F = 3.1$ meV and $x = 0.43$ at a gate voltage of 1.3 V. The fitting results show that a higher E_F is indeed accompanied by a larger x, which indicates that the contribution of the valley polarization of excitons is increased in the formation of trions at a higher background electron density. Furthermore, the fitting results show that E_F is increased by 1.2 meV as the gate voltage increases from 1 to 1.3 V. This increase is in good agreement with the dependence of the Fermi level on the gate voltage deduced from the device structure, which is calculated as $dE_F/dV_g = 3.42$ meV/V with use of the thickness of the bottom BN flake of 30 nm and the effective mass of the electron $m_e = 0.38m_0$ in ML WS_2 [22,55]. This further proves the validity of our quantitative model to analyze the polarization behaviors of trions in the nondegenerate-electron-density or weakly-degenerate-electron-density regime.

IV. CONCLUSION

In conclusion, we have investigated the polarization behaviors of the triplet trions and singlet trions in ML WS_2 under cw linearly-polarized-light excitation in out-of-plane magnetic fields. We observed that the magnetic field dependence of the polarization degree of the singlet trions is negative in the nondegenerate-electron-density regime and becomes positive in the weakly-degenerate-electron-density regime, while that of the triplet trions remains positive. In a bimolecular formation scenario where a trion is a bound state of an exciton and an electron, we proposed a model to quantitatively analyze the polarization behaviors of the triplet and singlet trions from the valley polarizations of the electrons and excitons. This work also reveals that for the development of ML-WS_2-based opto-valleytronic devices using trions as the carrier, samples with lower electron density are preferred as the helicity of the emissions under linearly-polarized-light excitation can be tuned more effectively.

The data that support the findings of this study are available from the corresponding author upon reasonable request.

ACKNOWLEDGMENTS

This work was supported by the Research Grants Council of the Hong Kong SAR under Grants No. 16307019, No. C7036-17W-1, No. C6008-20EF, and No. AoE/P-701/20, and in part by the National Natural Science Foundation of China (Grant No. 62074103). We acknowledge technical support from the Nano Fabrication Facility and the Materials Characterization and Preparation Facility.

The authors declare no conflict of interest.

APPENDIX A : POLARIZATION OF THE MEASUREMENT SYSTEM

To check the polarization selection of the magnetophotoluminescence system, we measured the polarization degrees of (a) the PL of CdSe quantum dots (QDs) and (b) the reflection of the excitation light from an Au electrode under different magnetic fields. A 593-nm, 2.091-eV laser with linear polarization was employed as the excitation light. The PL of the QDs has a peak energy of 1.98 eV which is close to that of the trions in ML WS_2. The results are plotted in Figs. 5(a) and 5(b), respectively. As shown in Fig. 5, both polarization degrees of the PL of the QDs and the reflected light of the excitation laser are close to zero under magnetic fields up to 16 T. This suggests that the polarization distortion from the measurement system is negligible.

APPENDIX B: TEMPERATURE DEPENDENT PL SPECTRA OF ML WS_2 (SAMPLE 1)

Figure 6 plots the temperature-dependent PL spectra of the ML WS_2 (sample 1) excited by a 593-nm, 2.091-eV linearly polarized laser. At 10 K, multipeaks can be identified, and the PL spectrum is dominated by the negative biexctions emission. As temperature increases, all peaks show red shift. In addition: (i) the relative intensities of the negative biexcitons emission, dark trions emission, and dark excitons emission decrease rapidly and

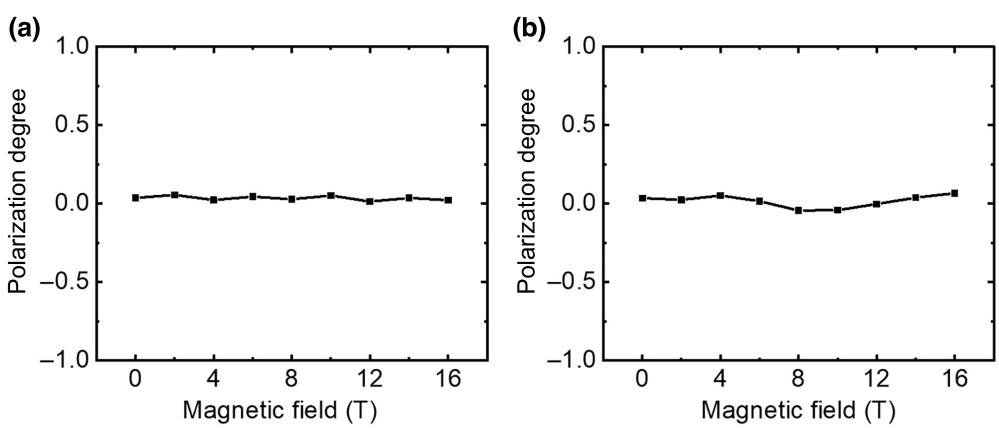

FIG. 5. Polarization degrees of (a) the PL spectra of CdSe QDs and (b) the reflection of the linearly polarized excitation laser from the Au film on the glass substrate, measured in the PPMS system equipped with an insert confocal microscope (Attocube) under different magnetic fields.

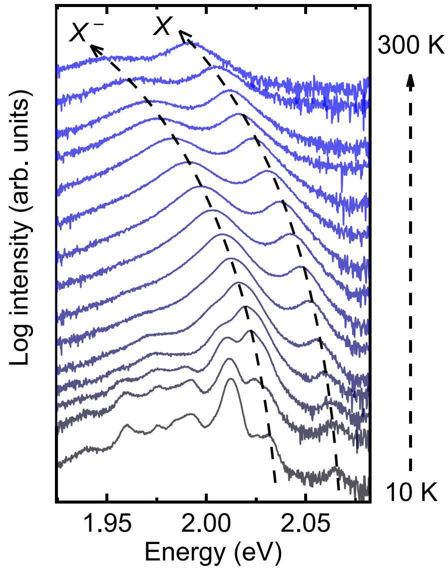

FIG. 6. Temperature-dependent PL spectra of ML WS_2 (sample 1) from 10 to 300 K with steps of 20 K in the range from 10 to 270 K, except for the last step (30 K) from 270 to 300 K. All the curves are normalized. The dashed lines are guides for the eye to show the evolution of the trion peak and the exciton peak, respectively. The curves are plotted on a base 10 logarithmic scale and shifted vertically.

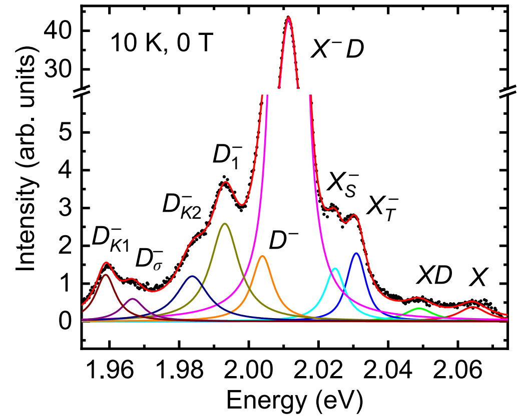

FIG. 7. PL spectrum (black dots) of sample 1 measured at 10 K and 0 T. The red line is the fitting curve obtained with use of multiple Voigt functions. The other colored lines represent the fitted multiple peaks.

vanish at temperatures above 130 K; (ii) the emission peaks of the singlet trions and triplet trions start to merge; meanwhile, the relative intensity of the trions emission increases; (iii) the relative intensity of the neutral exciton emission increases. At high temperatures above 130 K, the PL spectra are dominated by the emissions of trions and neutral excitons. The temperature-dependent evolution of the PL spectra verifies the assignment of the origin of the multipeaks in low-temperature PL spectrum.

APPENDIX C: AN EXAMPLE OF THE MULTIPEAK CURVE FITTING OF THE PL SPECTRA

The individual emission peaks can be decomposed from the PL spectrum by conducting curve fitting using a multi-Voigt function. Figure 7 shows an example of the curve fitting of the PL spectrum of sample 1 excited by a 593-nm, 2.091-eV linearly polarized laser at 10 K under zero magnetic field.

APPENDIX D: EVOLUTIONS OF THE PL SPECTRA IN THE TRION EMISSION RANGE UNDER MAGNETIC FIELDS

Figures 8(a) and 8(b) shows the σ^+ and σ^- PL spectra, respectively, of sample 1 in the energy range of trions emissions excited by a 593-nm, 2.091-eV linearly polarized laser under different magnetic fields. As the magnetic field increases from –16 T to 16 T: (i) in the σ^+ PL spectra, the intensity of the triplet (singlet) trions emission increases (decreases) and both triplet trion and singlet trion emission peaks show a red shift; (ii) in the σ^- PL spectra, the intensity of the triplet (singlet) trions emission decreases (increases) and both peak energies show a blue shift. In other words, as the magnetic field increases from –16 T to 16 T, the relative intensity of the low-energy component, that is, the σ^+ emission in positive magnetic field, of the triplet (singlet) trions increases (decreases). Therefore, the polarization degree of the triplet (singlet) trions emission shows a positive (negative) dependence on magnetic field.

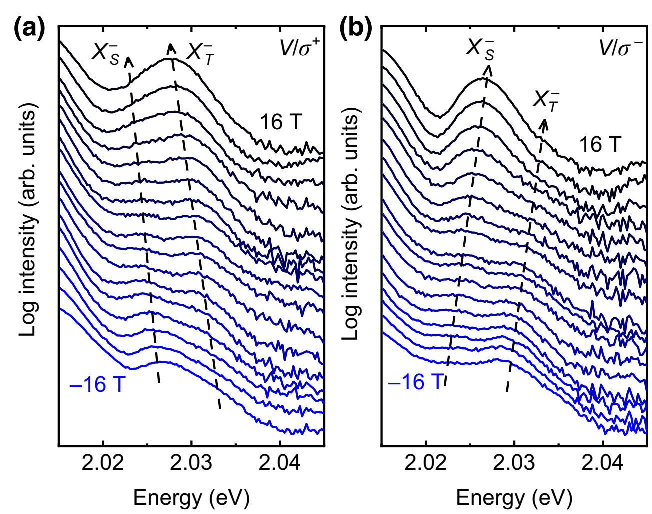

FIG. 8. Evolutions of PL spectra of triplet trions and singlet trions with (a) σ^+ detection and (b) σ^- detection measured at different magnetic fields from 16 to −16 T. The two dashed-line arrows are guides for the eye to show the peak evolution. The curves are plotted on a base 10 logarithmic scale and shifted vertically.

APPENDIX E: CURVE FITTINGS OF THE PL SPECTRA IN THE TRION AND NEGATIVE BIEXCITON RANGE UNDER DIFFERENT MAGNETIC FIELDS

Figure 9 shows the curve fittings of the σ^+ and σ^- PL spectra in the energy range of X_S^-, X_T^-, and X^-D emissions under magnetic fields of 0, 4, 8, and 12 T. The fitting results provide a clearer presentation on the magnetic field dependences of the triplet and singlet emissions discussed in Appendix D.

APPENDIX F: DEVICE STRUCTURE, GATE *I*-*V* CURVE, AND PL SPECTRUM OF SAMPLE 2

Figure 10(a) shows the schematic cross section of the gated ML-WS_2 device (sample 2). A *h*-BN layer with a thickness of ~30 nm was used as the dielectric layer. Figure 10(b) shows the gate *I*-*V* curve of sample 2. The gate current is below 100 pA with gate voltage up to 3 V. The low gate leakage current allows us to investigate the carrier density dependencies of the polarization behaviors of the trions. Figure 10(c) shows the σ^+ PL spectrum of sample 2 excited by a 593-nm, 2.091-eV laser with linearly polarization measured at 10 K. The trions emission from sample 2 shows clear double-peak feature and are the dominate peaks in the PL spectrum.

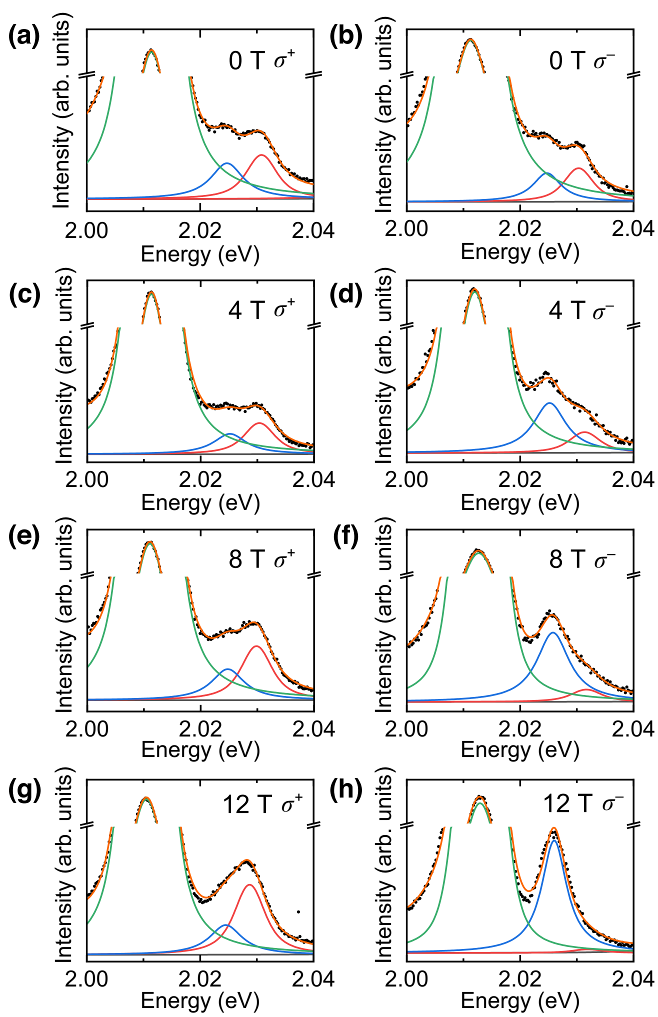

FIG. 9. Curve fittings of PL spectra in the energy range of X_S^-, X_T^-, and X^-D peaks measured under magnetic fields of 0, 4, 8, and 12 T with σ^+ and σ^- detection.

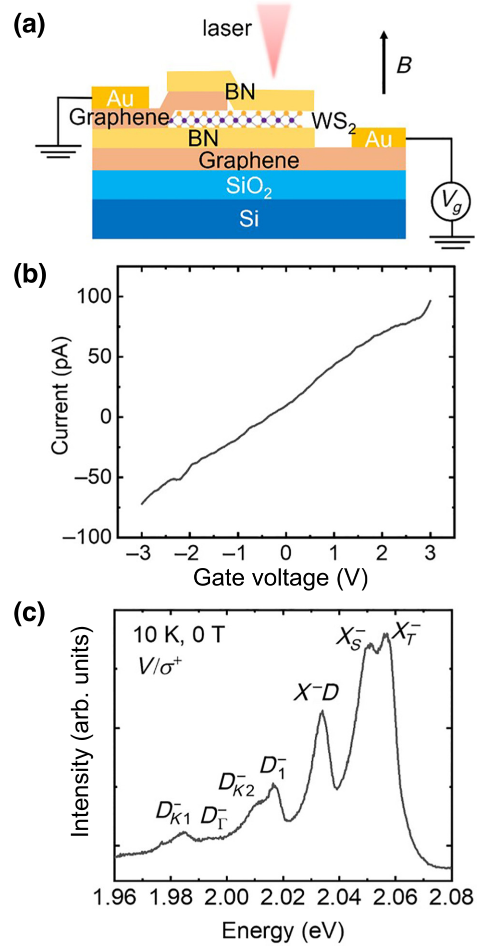

FIG. 10. (a) Cross section of the device and (b) gate *I*–*V* curve and (c) PL spectrum of sample 2 measured at 10 K under a magnetic field of 0 T with linear excitation and σ^+ detection.

[1] G. Wang, A. Chernikov, M. M. Glazov, T. F. Heinz, X. Marie, T. Amand, and B. Urbaszek, ColloquiumâĂŕ: Excitons in atomically thin transition metal dichalcogenides, Rev. Mod. Phys. **90**, 021001 (2018).

[2] T. Scrace, Y. Tsai, B. Barman, L. Schweidenback, A. Petrou, G. Kioseoglou, I. Ozfidan, M. Korkusinski, and P. Hawrylak, Magnetoluminescence and valley polarized state of a two-dimensional electron gas in WS_2 monolayers, Nat. Nanotechnol. **10**, 603 (2015).

[3] M. Barbone, A. R.-P. Montblanch, D. M. Kara, C. Palacios-Berraquero, A. R. Cadore, D. De Fazio, B. Pingault, E. Mostaani, H. Li, B. Chen, K. Watanabe, T. Taniguchi, S. Tongay, G. Wang, A. C. Ferrari, and M. Atatüre, Charge-tuneable biexciton complexes in monolayer WSe_2, Nat. Commun. **9**, 3721 (2018).

[4] P. Nagler, M. V. Ballottin, A. A. Mitioglu, M. V. Durnev, T. Taniguchi, K. Watanabe, A. Chernikov, C. Schüller, M. M. Glazov, P. C. M. Christianen, and T. Korn, Zeeman splitting and inverted polarization of biexciton emission in monolayer WS_2, Phys. Rev. Lett. **121**, 057402 (2018).

[5] S.-Y. Chen, T. Goldstein, T. Taniguchi, K. Watanabe, and J. Yan, Coulomb-bound four- and five-particle intervalley states in an atomically-thin semiconductor, Nat. Commun. **9**, 3717 (2018).

[6] S. Feng, C. Cong, S. Konabe, J. Zhang, J. Shang, Y. Chen, C. Zou, B. Cao, L. Wu, N. Peimyoo, B. Zhang, and T. Yu, Engineering valley polarization of monolayer WS_2: A physical doping approach, Small **15**, 1805503 (2019).

[7] M. He, P. Rivera, D. Van Tuan, N. P. Wilson, M. Yang, T. Taniguchi, K. Watanabe, J. Yan, D. G. Mandrus, H. Yu, H. Dery, W. Yao, and X. Xu, Valley phonons and exciton complexes in a monolayer semiconductor, Nat. Commun. **11**, 618 (2020).

[8] M. Zinkiewicz, T. Woźniak, T. Kazimierczuk, P. Kapuscinski, K. Oreszczuk, M. Grzeszczyk, M. Bartoš, K. Nogajewski, K. Watanabe, T. Taniguchi, C. Faugeras, P. Kossacki, M. Potemski, A. Babiński, and M. R. Molas, Excitonic complexes in n-doped WS_2 monolayer, Nano Lett. **21**, 2519 (2021).

[9] H. Li, G. Lu, Y. Wang, Z. Yin, C. Cong, Q. He, L. Wang, F. Ding, T. Yu, and H. Zhang, Mechanical exfoliation and characterization of single- and few-layer nanosheets of WSe_2, TaS_2, and $TaSe_2$, Small **9**, 1974 (2013).

[10] D. Xiao, G.-B. Liu, W. Feng, X. Xu, and W. Yao, Coupled spin and valley physics in monolayers of MoS_2 and other group-VI dichalcogenides, Phys. Rev. Lett. **108**, 196802 (2012).

[11] T. Cao, G. Wang, W. Han, H. Ye, C. Zhu, J. Shi, Q. Niu, P. Tan, E. Wang, B. Liu, and J. Feng, Valley-selective circular dichroism of monolayer molybdenum disulphide, Nat. Commun. **3**, 887 (2012).

[12] H. Zeng, J. Dai, W. Yao, D. Xiao, and X. Cui, Valley polarization in MoS_2 monolayers by optical pumping, Nat. Nanotechnol. **7**, 490 (2012).

[13] K. F. Mak, K. He, J. Shan, and T. F. Heinz, Control of valley polarization in monolayer MoS_2 by optical helicity, Nat. Nanotechnol. **7**, 8 (2012).

[14] T. P. Lyons, S. Dufferwiel, M. Brooks, F. Withers, T. Taniguchi, K. Watanabe, K. S. Novoselov, G. Burkard, and A. I. Tartakovskii, The valley Zeeman effect in inter- and intra-valley trions in monolayer WSe_2, Nat. Commun. **10**, 2330 (2019).

[15] G. Cheng, B. Li, Z. Jin, M. Zhang, and J. Wang, Observation of diffusion and drift of the negative trions in monolayer WS_2, Nano Lett. **21**, 6314 (2021).

[16] D. Sanvitto, F. Pulizzi, A. J. Shields, P. C. M. Christianen, S. N. Holmes, M. Y. Simmons, D. A. Ritchie, J. C. Maan, and M. Pepper, Observation of charge transport by negatively charged excitons, Science **294**, 837 (2001).

[17] K. Kheng, R. T. Cox, M. Y. d' Aubigné, F. Bassani, K. Saminadayar, and S. Tatarenko, Observation of negatively charged excitons X^- in semiconductor quantum wells, Phys. Rev. Lett. **71**, 1752 (1993).

[18] H. Buhmann, L. Mansouri, J. Wang, P. H. Beton, N. Mori, L. Eaves, M. Henini, and M. Potemski, Electron-concentration-dependent quantum-well luminescence: evidence for a negatively charged exciton, Phys. Rev. B **51**, 7969 (1995).

[19] M. T. Portella-Oberli, J. Berney, L. Kappei, F. Morier-Genoud, J. Szczytko, and B. Deveaud-Plédran, Dynamics of trion formation in $In_xGa_{1-x}As$ quantum wells, Phys. Rev. Lett. **102**, 096402 (2009).

[20] D. K. Efimkin and A. H. MacDonald, Many-body theory of trion absorption features in two-dimensional semiconductors, Phys. Rev. B **95**, 035417 (2017).

[21] C. Robert, S. Park, F. Cadiz, L. Lombez, L. Ren, H. Tornatzky, A. Rowe, D. Paget, F. Sirotti, M. Yang, D. Van Tuan, T. Taniguchi, B. Urbaszek, K. Watanabe, T. Amand, H. Dery, and X. Marie, Spin/valley pumping of resident electrons in WSe_2 and WS_2 monolayers, Nat. Commun. **12**, 1 (2021).

[22] E. Liu, J. van Baren, Z. Lu, T. Taniguchi, K. Watanabe, D. Smirnov, Y.-C. Chang, and C. H. Lui, Exciton-polaron Rydberg states in monolayer $MoSe_2$ and WSe_2, Nat. Commun. **12**, 6131 (2021).

[23] X. Xu, W. Yao, D. Xiao, and T. F. Heinz, Spin and pseudospins in layered transition metal dichalcogenides, Nat. Phys. **10**, 343 (2014).

[24] G. Aivazian, Z. Gong, A. M. Jones, R.-L. Chu, J. Yan, D. G. Mandrus, C. Zhang, D. Cobden, W. Yao, and X. Xu, Magnetic control of valley pseudospin in monolayer WSe_2, Nat. Phys. **11**, 148 (2015).

[25] F. Pizzocchero, L. Gammelgaard, B. S. Jessen, J. M. Caridad, L. Wang, J. Hone, P. Bøggild, and T. J. Booth, The hot pick-up technique for batch assembly of van der Waals heterostructures, Nat. Commun. **7**, 11894 (2016).

[26] J. I.-J. Wang, Y. Yang, Y.-A. Chen, K. Watanabe, T. Taniguchi, H. O. H. Churchill, and P. Jarillo-Herrero, Electronic transport of encapsulated graphene and WSe_2 devices fabricated by pick-up of prepatterned hBN, Nano Lett. **15**, 1898 (2015).

[27] D. Vaclavkova, J. Wyzula, K. Nogajewski, M. Bartos, A. O. Slobodeniuk, C. Faugeras, M. Potemski, and M. R. Molas, Singlet and triplet trions in WS_2 monolayer encapsulated in hexagonal boron nitride, Nanotechnology **29**, 325705 (2018).

[28] G. Plechinger, P. Nagler, A. Arora, A. Granados del Águila, M. V. Ballottin, T. Frank, P. Steinleitner, M. Gmitra, J. Fabian, P. C. M. Christianen, R. Bratschitsch, C. Schüller, and T. Korn, Excitonic valley effects in monolayer WS_2 under high magnetic fields, Nano Lett. **16**, 7899 (2016).

[29] G. Plechinger, P. Nagler, A. Arora, R. Schmidt, A. Chernikov, A. G. del Águila, P. C. M. Christianen, R. Bratschitsch, C. Schüller, and T. Korn, Trion fine structure and coupled spin–valley dynamics in monolayer tungsten disulfide, Nat. Commun. **7**, 12715 (2016).

[30] Z. Ye, L. Waldecker, E. Y. Ma, D. Rhodes, A. Antony, B. Kim, X.-X. Zhang, M. Deng, Y. Jiang, Z. Lu, D. Smirnov, K. Watanabe, T. Taniguchi, J. Hone, and T. F. Heinz, Efficient generation of neutral and charged biexcitons in

encapsulated WSe_2 monolayers, Nat. Commun. **9**, 3718 (2018).
[31] Z. Li, T. Wang, Z. Lu, C. Jin, Y. Chen, Y. Meng, Z. Lian, T. Taniguchi, K. Watanabe, S. Zhang, D. Smirnov, and S.-F. Shi, Revealing the biexciton and trion-exciton complexes in BN encapsulated WSe_2, Nat. Commun. **9**, 3719 (2018).
[32] G. A. Prando, M. E. Severijnen, I. D. Barcelos, U. Zeitler, P. C. M. Christianen, F. Withers, and Y. Galvão Gobato, Revealing excitonic complexes in monolayer WS_2 on talc dielectric, Phys. Rev. Appl. **16**, 064055 (2021).
[33] Z. Ye, T. Cao, K. O'Brien, H. Zhu, X. Yin, Y. Wang, S. G. Louie, and X. Zhang, Probing excitonic dark states in single-layer tungsten disulphide, Nature **513**, 214 (2014).
[34] Z. Li, T. Wang, Z. Lu, M. Khatoniar, Z. Lian, Y. Meng, M. Blei, T. Taniguchi, K. Watanabe, S. A. McGill, S. Tongay, V. M. Menon, D. Smirnov, and S.-F. Shi, Direct observation of gate-tunable dark trions in monolayer WSe_2, Nano Lett. **19**, 6886 (2019).
[35] E. Liu, J. van Baren, Z. Lu, M. M. Altaiary, T. Taniguchi, K. Watanabe, D. Smirnov, and C. H. Lui, Gate tunable dark trions in monolayer WSe_2, Phys. Rev. Lett. **123**, 027401 (2019).
[36] X.-X. Zhang, T. Cao, Z. Lu, Y.-C. Lin, F. Zhang, Y. Wang, Z. Li, J. C. Hone, J. A. Robinson, D. Smirnov, S. G. Louie, and T. F. Heinz, Magnetic brightening and control of dark excitons in monolayer WSe_2, Nat. Nanotechnol. **12**, 883 (2017).
[37] M. Zinkiewicz, A. O. Slobodeniuk, T. Kazimierczuk, P. Kapuściński, K. Oreszczuk, M. Grzeszczyk, M. Bartos, K. Nogajewski, K. Watanabe, T. Taniguchi, C. Faugeras, P. Kossacki, M. Potemski, A. Babiński, and M. R. Molas, Neutral and charged dark excitons in monolayer WS_2, Nanoscale **12**, 18153 (2020).
[38] Z. Li, T. Wang, C. Jin, Z. Lu, Z. Lian, Y. Meng, M. Blei, S. Gao, T. Taniguchi, K. Watanabe, T. Ren, S. Tongay, L. Yang, D. Smirnov, T. Cao, and S.-F. Shi, Emerging photoluminescence from the dark-exciton phonon replica in monolayer WSe_2, Nat. Commun. **10**, 2469 (2019).
[39] E. Liu, J. van Baren, T. Taniguchi, K. Watanabe, Y.-C. Chang, and C. H. Lui, Valley-selective chiral phonon replicas of dark excitons and trions in monolayer WSe_2, Phys. Rev. Res. **1**, 032007 (2019).
[40] J. Jadczak, L. Bryja, J. Kutrowska-Girzycka, P. Kapuściński, M. Bieniek, Y.-S. Huang, and P. Hawrylak, Room temperature multi-phonon upconversion photoluminescence in monolayer semiconductor WS_2, Nat. Commun. **10**, 107 (2019).
[41] Z. Li, T. Wang, C. Jin, Z. Lu, Z. Lian, Y. Meng, M. Blei, M. Gao, T. Taniguchi, K. Watanabe, T. Ren, T. Cao, S. Tongay, D. Smirnov, L. Zhang, and S.-F. Shi, Momentum-dark intervalley exciton in monolayer tungsten diselenide brightened via chiral phonon, ACS Nano **13**, 14107 (2019).
[42] A. A. Mitioglu, P. Plochocka, J. N. Jadczak, W. Escoffier, G. L. J. A. Rikken, L. Kulyuk, and D. K. Maude, Optical manipulation of the exciton charge state in single-layer tungsten disulfide, Phys. Rev. B **88**, 245403 (2013).
[43] E. Liu, J. van Baren, C.-T. Liang, T. Taniguchi, K. Watanabe, N. M. Gabor, Y.-C. Chang, and C. H. Lui, Multipath optical recombination of intervalley dark excitons and trions in monolayer WSe_2, Phys. Rev. Lett. **124**, 196802 (2020).
[44] J. Förste, N. V. Tepliakov, S. Yu. Kruchinin, J. Lindlau, V. Funk, M. Förg, K. Watanabe, T. Taniguchi, A. S. Baimuratov, and A. Högele, Exciton g-factors in monolayer and bilayer WSe_2 from experiment and theory, Nat. Commun. **11**, 4539 (2020).
[45] M. Koperski, M. R. Molas, A. Arora, K. Nogajewski, M. Bartos, J. Wyzula, D. Vaclavkova, P. Kossacki, and M. Potemski, Orbital, spin and valley contributions to zeeman splitting of excitonic resonances in $MoSe_2$, WSe_2 and WS_2 monolayers, 2D Mater. **6**, 015001 (2018).
[46] T. Deilmann, P. Krüger, and M. Rohlfing, Ab initio studies of exciton g factors: Monolayer transition metal dichalcogenides in magnetic fields, Phys. Rev. Lett. **124**, 226402 (2020).
[47] T. Woźniak, P. E. Faria Junior, G. Seifert, A. Chaves, and J. Kunstmann, Exciton g Factors of van der Waals heterostructures from first-principles calculations, Phys. Rev. B **101**, 235408 (2020).
[48] G. Wang, L. Bouet, D. Lagarde, M. Vidal, A. Balocchi, T. Amand, X. Marie, and B. Urbaszek, Valley dynamics probed through charged and neutral exciton emission in monolayer WSe_2, Phys. Rev. B **90**, 075413 (2014).
[49] T. Yu and M. W. Wu, Valley depolarization due to intervalley and intravalley electron-hole exchange interactions in monolayer MoS_2, Phys. Rev. B **89**, 205303 (2014).
[50] A. Singh, K. Tran, M. Kolarczik, J. Seifert, Y. Wang, K. Hao, D. Pleskot, N. M. Gabor, S. Helmrich, N. Owschimikow, U. Woggon, and X. Li, Long-lived valley polarization of intravalley trions in monolayer WSe_2, Phys. Rev. Lett. **117**, 257402 (2016).
[51] A. Singh, G. Moody, K. Tran, M. E. Scott, V. Overbeck, G. Berghäuser, J. Schaibley, E. J. Seifert, D. Pleskot, N. M. Gabor, J. Yan, D. G. Mandrus, M. Richter, E. Malic, X. Xu, and X. Li, Trion formation dynamics in monolayer transition metal dichalcogenides, Phys. Rev. B **93**, 041401 (2016).
[52] F. Gao, Y. Gong, M. Titze, R. Almeida, P. M. Ajayan, and H. Li, Valley trion dynamics in monolayer $MoSe_2$, Phys. Rev. B **94**, 245413 (2016).
[53] C. Lee, B. G. Jeong, S. H. Kim, D. H. Kim, S. J. Yun, W. Choi, S.-J. An, D. Lee, Y.-M. Kim, K. K. Kim, S. M. Lee, and M. S. Jeong, Investigating heterogeneous defects in single-crystalline WS_2 via tip-enhanced Raman spectroscopy, Npj 2D Mater. Appl. **6**, 1 (2022).
[54] B. Schuler, J.-H. Lee, C. Kastl, K. A. Cochrane, C. T. Chen, S. Refaely-Abramson, S. Yuan, E. Van Veen, R. Roldán, N. J. Borys, R. J. Koch, S. Aloni, A. M. Schwartzberg, D. F. Ogletree, J. B. Neaton, and A. Weber-Bargioni, How substitutional point defects in two-dimensional WS_2 induce charge localization, spin–orbit splitting, and strain, ACS Nano **13**, 10520 (2019).
[55] E. Mostaani, M. Szyniszewski, C. H. Price, R. Maezono, M. Danovich, R. J. Hunt, N. D. Drummond, and V. I. Fal'ko, Diffusion quantum Monte Carlo Study of excitonic complexes in two-dimensional transition-metal dichalcogenides, Phys. Rev. B **96**, 075431 (2017).